

Reaction Sintering of Mexican Dolomite – Zircon Mixtures

J. L. RODRÍGUEZ-GALICIA¹, B. FERNÁNDEZ-ARGUIJO¹, J. C. RENDÓN-ANGELES¹, P. PENA², J. F. VALLE-FUENTES² AND J. LÓPEZ-CUEVAS¹

¹ CINVESTAV-IPN, Unidad Saltillo, Carretera Saltillo-Monterrey, Km. 13.5, Ramos Arizpe, Coahuila, Mexico.

² Instituto de Cerámica y Vidrio, C.S.I.C., c/ Kelsen nº 5, Cantoblanco, 28049, Madrid, Spain.

The present work has been conducted aiming to develop additional phase [Ca₃SiO₅, Ca₂SiO₄ and/or Ca₃Mg(SiO₄)₂]-bonded magnesia refractory materials via reaction sintering of dolomite-zircon mixtures, employing a Mexican dolomite containing an excess of 3 wt% of CaCO₃. The study was based on phase equilibrium data extracted from the quaternary system CaO – MgO – SiO₂ – ZrO₂, to put it more precisely, base on the projection from the MgO-apex of the liquidus surface of the primary crystallization volume of MgO onto the opposite face of the above mentioned quaternary system. The refractory materials designed within this system were obtained by attrition milling, followed by cold isostatic pressing and high temperature reaction sintering. All initial and produced materials were characterized by ICP-AES, XRF, XRD, SEM-EDX, DTA and TG analyses. The results obtained indicated that reaction sintering of dolomite-zircon mixtures is an interesting route to produce MgO-CaZrO₃-additional phase refractory materials.

Keywords: Dolomite; MgO-based refractories; Reaction Sintering; Zircon..

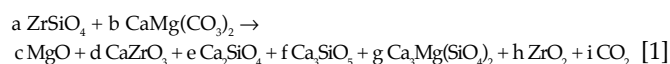
Sinterización reactiva de mezclas de dolomita mexicana – circón

El propósito de este trabajo ha sido obtener materiales refractarios de magnesia, aglomerados con una fase adicional [Ca₃SiO₅, Ca₂SiO₄ y/o Ca₃Mg(SiO₄)₂], mediante la sinterización reactiva de mezclas de dolomita-circón, empleando para ello una dolomita mexicana que contiene un exceso de 3% en peso de CaCO₃. El estudio se basa en la información relativa al equilibrio de fases del sistema CaO – MgO – SiO₂ – ZrO₂. En concreto se usa la proyección, desde el vértice del MgO, de la superficie de liquidus del volumen de cristalización primaria de este, hacia la cara opuesta de sistema cuaternario. Los materiales refractarios diseñados se han obtenido por molienda de atrición, seguida de un prensado isostático en frío y sinterización reactiva a alta temperatura. Todos los materiales, iniciales y finales, han sido caracterizados mediante ICP-AES, FRX, DRX, MEB-EDX, ATD y TG. Los resultados obtenidos indican que la sinterización reactiva de las mezclas de dolomita-circón es una ruta interesante para la producción de materiales refractarios de MgO-CaZrO₃-fase adicional.

Palabras clave: Dolomita; refractarios de magnesia; sinterización reactiva; circón.

1. INTRODUCTION

The use of naturally occurring minerals is an attractive alternative for the production of low cost, MgO-based, high temperature structural materials (1-5). For instance, Spanish dolomite [CaMg(CO₃)₂] and zircon (ZrSiO₄) have been employed to develop refractory materials with good mechanical and corrosive properties, based on the quaternary system CaO – MgO – SiO₂ – ZrO₂, considering particularly the MgO-CaZrO₃-Ca₂SiO₄ isoplethal section and primary crystallization volume of MgO (5). The reaction products obtained were in accordance with general chemical equation 1:



In the present work, a Mexican dolomite containing an excess of 3 wt% of CaCO₃ was employed to develop additional phase [Ca₃SiO₅, Ca₂SiO₄ and/or Ca₃Mg(SiO₄)₂]-bonded magnesia materials with potential application as refractory matrixes, via reaction sintering of dolomite-zircon mixtures. An excess of CaCO₃ constitutes a fundamental variable since it has a determinant effect on the chemical composition of

the reaction products, as well as on the final mechanical and corrosion properties of the refractory materials (2, 5).

2. EXPERIMENTAL PROCEDURE

The raw materials used were mineral zircon (American Minerals, Smurfit-Stone, USA) and dolomite (Química del Rey, Peñoles, México). Chemical analyses of both raw materials were carried out by inductively coupled plasma (ICP) and X-ray fluorescence (XRF). The grain size distribution of dolomite and zircon was determined by laser scattering. The studied compositions were formulated on the basis of information extracted from the quaternary system CaO-MgO-ZrO₂-SiO₂ [6] (Fig. 1a), considering the MgO primary crystallization, field in the solid state compatibility plane CaO-SiO₂-ZrO₂ (Fig. 1b and c). Five compositions lying on a straight line joining the dolomite and zircon compositions (Fig. 1a) were investigated. This line crossed three tetrahedral regions whose boundaries limited the zones of thermodynamic stability of several high-temperature phases. Region I corresponded to subsystem MgO-CaZrO₃-Ca₂SiO₄-Ca₃SiO₅, Region II corresponded to

subsystem $\text{MgO-CaZrO}_3\text{-Ca}_2\text{SiO}_4\text{-Ca}_3\text{Mg}(\text{SiO}_4)_2$, and Region III corresponded to subsystem $\text{MgO-CaZrO}_3\text{-Ca}_3\text{Mg}(\text{SiO}_4)_2\text{-ZrO}_2$. Only regions II and III were of interest in the present work due to the temperature range considered. An equation that satisfies the phases limited by the tetrahedral boundaries was formulated for each one of these regions. The required $\text{CaMg}(\text{CO}_3)_2/\text{ZrSiO}_4$ ratios were determined from the stoichiometric proportions indicated by equation 2 for region II and by equation 3 for region III (Fig. 1b):

$$(1 + x) \text{ZrSiO}_4 + (3 + 2x) \text{CaO} \cdot \text{MgO} \rightarrow (3 + x) \text{MgO} + (1 + x) \text{CaZrO}_3 + (1 - x) \text{Ca}_2\text{SiO}_4 + x \text{Ca}_3\text{Mg}(\text{SiO}_4)_2 \quad [2]$$

$$2 \text{ZrSiO}_4 + (5 - 2x) \text{CaO} \cdot \text{MgO} \rightarrow (4 - 2x) \text{MgO} + 2(1 - x) \text{CaZrO}_3 + 2x \text{ZrO}_2 + \text{Ca}_3\text{Mg}(\text{SiO}_4)_2 \quad [3]$$

where $0 \leq X \leq 1$. The studied molar compositions varied from $X=0$ to $X=1$, at intervals of 0.25. Throughout this paper, the compositions of all minerals and mineral mixtures are given in weight percentages. Considering the excess of 3 % of CaCO_3 in the Mexican dolomite, for region II composition $X = 0$ corresponded to a mineral mixture having 27.3% zircon and 72.7% dolomite, while composition $X = 1$ corresponded to a mixture with 30.6% zircon and 69.4% dolomite. Similarly, for region III composition $X = 0$ corresponded to 30.59% zircon and 69.41% dolomite, while composition $X = 1$ corresponded to 41.1% zircon and 58.9% dolomite. The rest of the studied compositions had zircon and dolomite weight proportions falling within these ranges.

All regions have different invariant points, which constitute important information needed to establish the sintering temperature for the studied compositions. According to the quaternary system (Fig. 1a), for regions II and III liquid formation starts at 1555 and 1475°C, respectively.

The processing route followed to produce the refractory materials included the five steps: a) conditioning of raw materials, b) high energy milling, c) cold isostatic pressing, d) firing at high temperature and, finally, e) microstructural and phase characterization of the obtained materials by X ray diffraction (XRD), scanning electron microscopy (SEM-EDX), differential thermal analyses (DTA) and thermogravimetric analyses (TG) (7,8).

Dolomite-zircon mixtures were milled and homogenized by attrition milling, with MgO-partially stabilised zirconia balls in water media, for 4 hours; resulting in an average particle size of 1 μm . Longer milling times did not reduce significantly the average particle size. The particle size distribution was determined by the laser scattering method (COULTER LS-100Q apparatus) and the grain size in the microstructure was determined by the line intersection size method [9]. After milling, bars with a diameter of ~ 5 mm were obtained by cold isostatic pressing at 200 MPa. Subsequently, the specimens were fired in a high temperature furnace at temperatures in the range of 1400-1600°C. The heating rate employed was 2°C·min⁻¹, with a holding time of 2 h at the treatment temperature. Fired products thus obtained were characterized by scanning

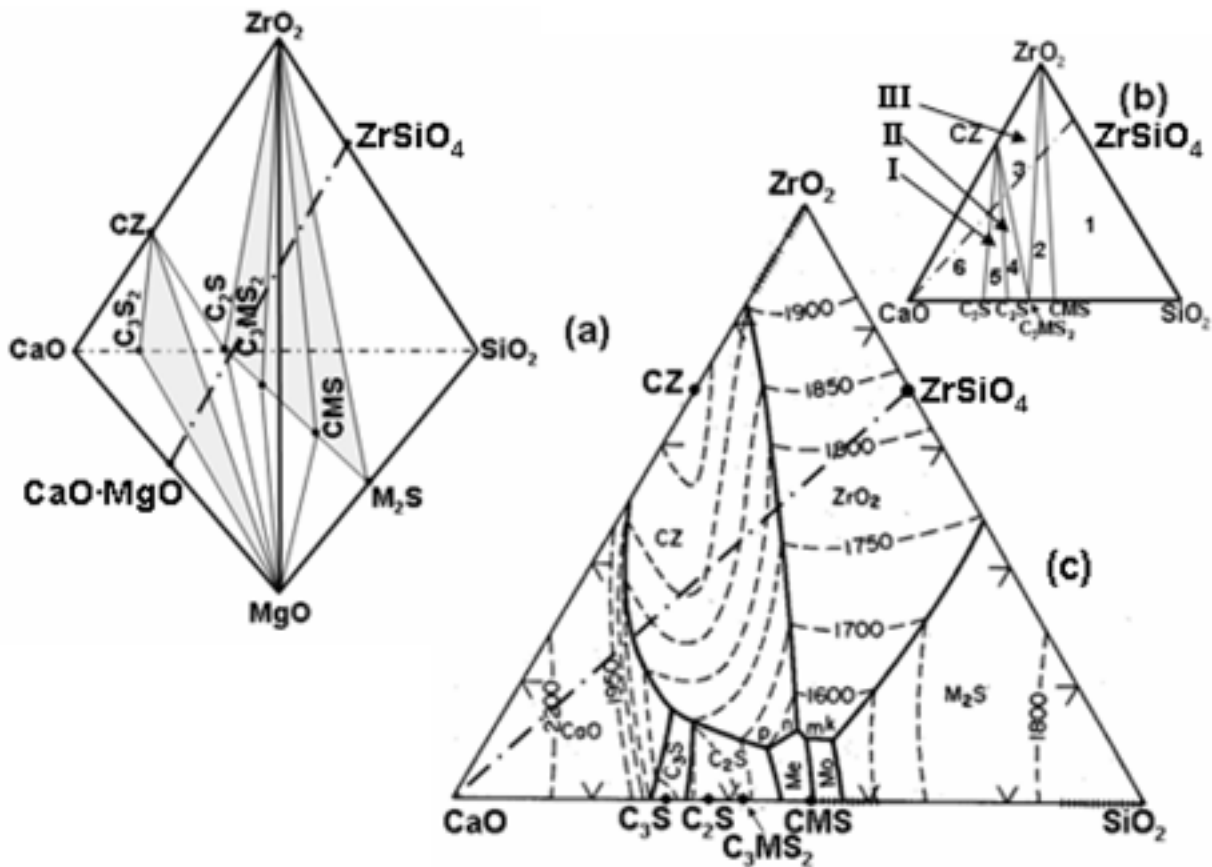


Fig. 1.- (a) Phase diagram of MgO-CaO-ZrO₂-SiO₂ system with a diagrammatic representation of the intersection between the solid state compatibility planes and the dolomite-zircon formulation line; (b) projected subsolidus assemblage showing phase combinations coexisting with MgO in the solid state; (c) projection from the MgO-apex onto the opposite face of quaternary tetrahedron CaO- ZrO₂-SiO₂ showing secondary phase crystallizing during freezing from CaO-MgO-ZrO₂-SiO₂ mixtures and isotherms on the liquidus surface [5, 6]. For simplicity, solid phases given in the figures are described by abbreviated formulas, i.e. CaO = C, SiO₂ = S, CaZrO₃ = CZ and Ca₂SiO₄ = C₂S.

electron microscopy (Phillips XL30 ESEM) coupled to energy dispersive X-ray analysis (EDX). X-ray powder diffraction patterns of the fired materials were obtained using a Siemens 5000 diffractometer, with nickel-filtered Cu- k_{α} radiation, operating at 50 kV and 30 mA. Diffraction patterns were recorded in the 2θ range of 10-70°. The thermal analyses were carried out up to a maximum temperature of 1200°C, using a heating and a cooling rate of 5°C/min, employing a Pyris Diamond TG/DTA SII Perkin Elmer apparatus.

3. RESULTS AND DISCUSSION

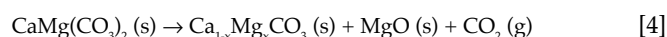
3.1 Chemical composition of raw minerals

The chemical analyses of dolomite indicated that this mineral was composed by 32.4% CaO, 20.1% MgO, 0.14% Al_2O_3 , 0.12% SiO_2 , 0.003% P_2O_5 , 0.084% SO_3 , 0.013% K_2O , 0.012% MnO_2 , 0.13% Fe_2O_3 , and 0.01% SrO, with a loss on ignition of 47.2% at 900°C. XRD analyses indicated that the powder consisted essentially of dolomite and a small amount of calcite. These results are in good agreement with the chemical analyses. In terms of its phase composition, the analyzed dolomite contained 3% $CaCO_3$, ~ 96% $CaMg(CO_3)_2$, and 0.5% of other inorganic constituents. The chemical composition of zircon was 0.21% CaO, 0.033% MgO, 0.61% Al_2O_3 , 31.4% SiO_2 , 0.002% K_2O , 0.011% Na_2O , 67.6% ZrO_2+HfO_2 and 0.12% Fe_2O_3 . This chemical composition is very close to the stoichiometric composition of $ZrSiO_4$, which was confirmed by XRD analysis since significant impurities were not detected by this technique.

3.2 Thermal behavior of mineral mixtures

Figure 2 shows DTA and TG curves obtained for composition X = 0 in regions I, II and III. The DTA plots (Fig. 2a) exhibited two endothermic peaks, which were located at temperature ranges of 743 - 979°C, 743 - 1006°C and 740

- 988°C, for regions I, II and III, respectively. The endothermic peak located at higher temperature is not well defined because the DTA analyses were carried out by using milled and non compacted dolomite. These endothermic peaks are characteristic of dolomite decomposition at low CO_2 pressure or in powdered state (10). In compacted samples dolomite decomposes in two well defined steps. The first one takes place at 775°C, yielding calcite and periclase (MgO) accompanied by a release of gaseous CO_2 (Eq. 4). The second one occurs at 870°C and it is due to the decomposition of calcite (Eq. 5):



When the CO_2 partial pressure decreases, the endotherm at 775°C is shifted to higher temperatures and the endotherm at 870°C moves in the opposite direction, until the two endotherms merge at pressures < 260 mmHg and the decomposition of dolomite proceeds in two steps to yield CaO, MgO and CO_2 (11, 12).

The TG curves (Fig. 2b) indicated a weight loss of 66.1%, 63.3% and 62.9% for regions I, II and III, respectively. This sequence of diminution in the weight loss was associated with a corresponding decrease in the content of carbonated materials, particularly $CaCO_3$ in excess, in the mineral mixtures prepared for each region.

3.3 Crystalline phases formed in the sintered samples

Figure 3 shows the XRD patterns of sintered dolomite - zircon mixtures, indicating, in general, the formation of the phases predicted by the quaternary phase diagram. Fig. 3a corresponds to the XRD patterns for region II at 1550°C, revealing the presence of five crystalline phases: $CaZrO_3$, Ca_2SiO_4 , $Ca_3Mg(SiO_4)_2$ (merwinite), $CaSiO_3$ (wollastonite) and MgO. Except for composition X = 0.5, the main phases present in the samples were $CaZrO_3$ and MgO, plus a small

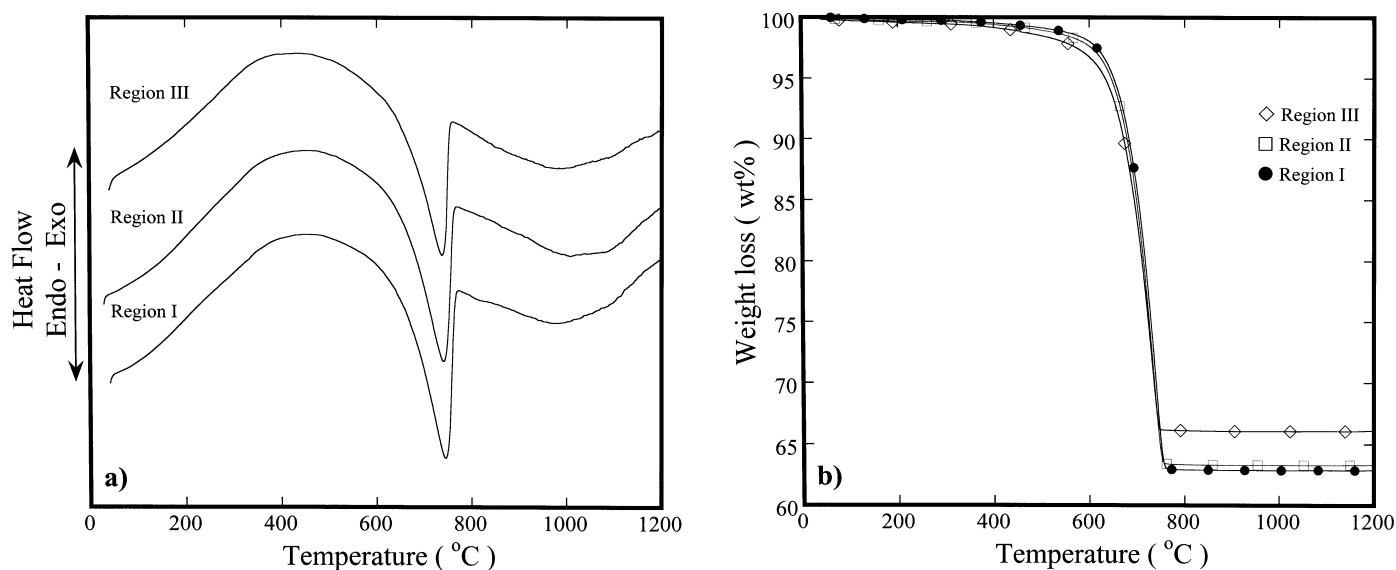


Fig. 2.- Thermal behavior of green compacted samples: (a) DTA plot, (b) TG plot. Heating rate 2°C/min⁻¹.

amount of $\text{Ca}_3\text{Mg}(\text{SiO}_4)_2$. Ca_2SiO_4 was detected only in the sample of composition $X = 0$, while CaSiO_3 was found only in compositions $X = 0.25$ and $X = 0.5$. The formation of the latter phase was not predicted by the quaternary phase diagram, and it is likely due to the presence of an excess of calcite, which reacts partially with zircon. As can be noticed, the amount of CaZrO_3 and MgO phases decreases gradually from $X = 0$ to $X = 0.5$, achieving a minimum relative intensity at the latter composition. This is accompanied by the disappearance of Ca_2SiO_4 , with the simultaneous appearance of CaSiO_3 , at composition $X = 0.25$. Then, the amount of the latter phase increases, achieving a maximum at $X = 0.5$ and becoming the main constituent of the material at this composition. Later on, the amount of the CaZrO_3 and MgO phases increases sharply for $X = 0.75$, the former phase becoming again the main constituent of the material. Lastly, at composition $X = 1$, the amount of CaZrO_3 and MgO phases remains unchanged with respect to the previous composition. The relative proportion of the $\text{Ca}_3\text{Mg}(\text{SiO}_4)_2$ phase remains nearly constant in all cases.

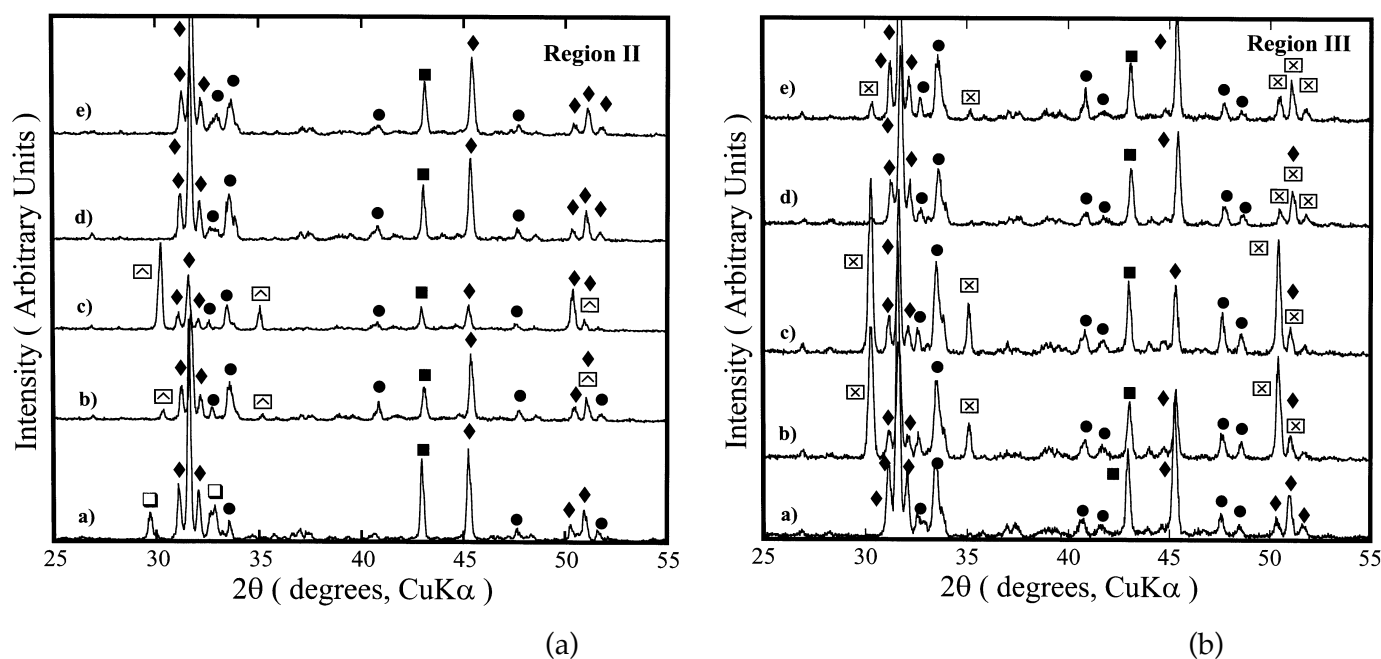


Fig. 3.- XRD patterns of sintered dolomite – zircon mixtures, for regions II and III and compositions a) $X = 0$, b) $X = 0.25$, c) $X = 0.5$, d) $X = 0.75$ and e) $X = 1$. Key: (□) Ca_2SiO_4 , (●) $\text{Ca}_3\text{Mg}(\text{SiO}_4)_2$, (▲) CaSiO_3 , (◆) CaZrO_3 , (■) MgO and (x) ZrO_2 .

Fig. 3b corresponds to the XRD patterns for region III at 1450 or 1500°C, revealing the presence of four main crystalline phases: $\text{Ca}_3\text{Mg}(\text{SiO}_4)_2$, CaZrO_3 , MgO and ZrO_2 . All four phases were found in compositions with $X > 0$, but ZrO_2 was not detected for composition $X = 0$. These results are in accordance with the predictions made based on the quaternary phase diagram. As can be appreciated, the amount of the CaZrO_3 phase decreases gradually from $X = 0$ to $X = 0.5$. Then, it increases sharply for $X = 0.75$, increasing slightly again for $X = 1$. In contrast, the amount of the $\text{Ca}_3\text{Mg}(\text{SiO}_4)_2$ and ZrO_2 phases increases gradually from $X = 0$ to $X = 0.5$. Then, it decreases sharply for $X = 0.75$, increasing slightly again for $X = 1$. The proportion of MgO is slightly larger for $X = 0$ with respect to the other compositions, all of which have a similar MgO level.

3.4 Microstructural evolution during reaction sintering

Figs. 4a and 4b show micrographs of two samples with molar compositions $X = 0$ and $X = 1$, respectively, corresponding to region II sintered at 1550°C. The first sample (Fig. 4a) shows four phases. Phase 1 has a white color and a rounded morphology, with a particle size of $\sim 1\text{-}5\ \mu\text{m}$. EDS analyses conducted on particles of this phase indicated a molar ratio $\text{Ca}:\text{Zr} = 50.6(9):49.4(9)$, corresponding to the chemical formula CaZrO_3 . Phase 2 is also rounded and has a dark gray color, with a particle size of $\sim 2\ \mu\text{m}$. This phase is composed basically by Mg and oxygen, corresponding to MgO . Phases 3 and 4 have a similar light gray color, which is slightly darker for the case of phase 3. The latter phase constitutes the matrix of the material and presents a molar ratio $\text{Ca}:\text{Mg}:\text{Si} = 50.1(9):33.4(9):16.6(9)$, corresponding to $\text{Ca}_3\text{Mg}(\text{SiO}_4)_2$. Phase 4 has a particle size of $\sim 5\text{-}10\ \mu\text{m}$ and presents a molar ratio $\text{Ca}:\text{Si} = 65.3(9):34.7(9)$, corresponding to Ca_2SiO_4 . All phases are homogeneously distributed, with similar relative proportions in the sample.

These crystalline phases correspond to those predicted from the solid state compatibility plane $\text{CaO-SiO}_2\text{-ZrO}_2$ in region II within the quaternary system $\text{CaO-MgO-ZrO}_2\text{-SiO}_2$ (Fig. 1). Despite of having detected, by XRD, the presence of CaSiO_3 for $X = 0.25$ and $X = 0.5$, this phase was not identified in the MEB, perhaps due to its small amount.

The second sample (Fig. 4b) shows only the presence of CaZrO_3 , MgO and $\text{Ca}_3\text{Mg}(\text{SiO}_4)_2$ phases. The first two phases has a particle size of 2-5, 5-20 μm , respectively, all of which are less abundant but considerably larger in this specimen than in the sample of Fig. 4a. CaZrO_3 shows a blocky morphology, MgO is composed by rounded particles and $\text{Ca}_3\text{Mg}(\text{SiO}_4)_2$ constitutes the matrix of the material. All phases are homogeneously distributed and their relative proportions decrease in the sequence $\text{Ca}_3\text{Mg}(\text{SiO}_4)_2 \rightarrow \text{CaZrO}_3 \rightarrow \text{MgO}$.

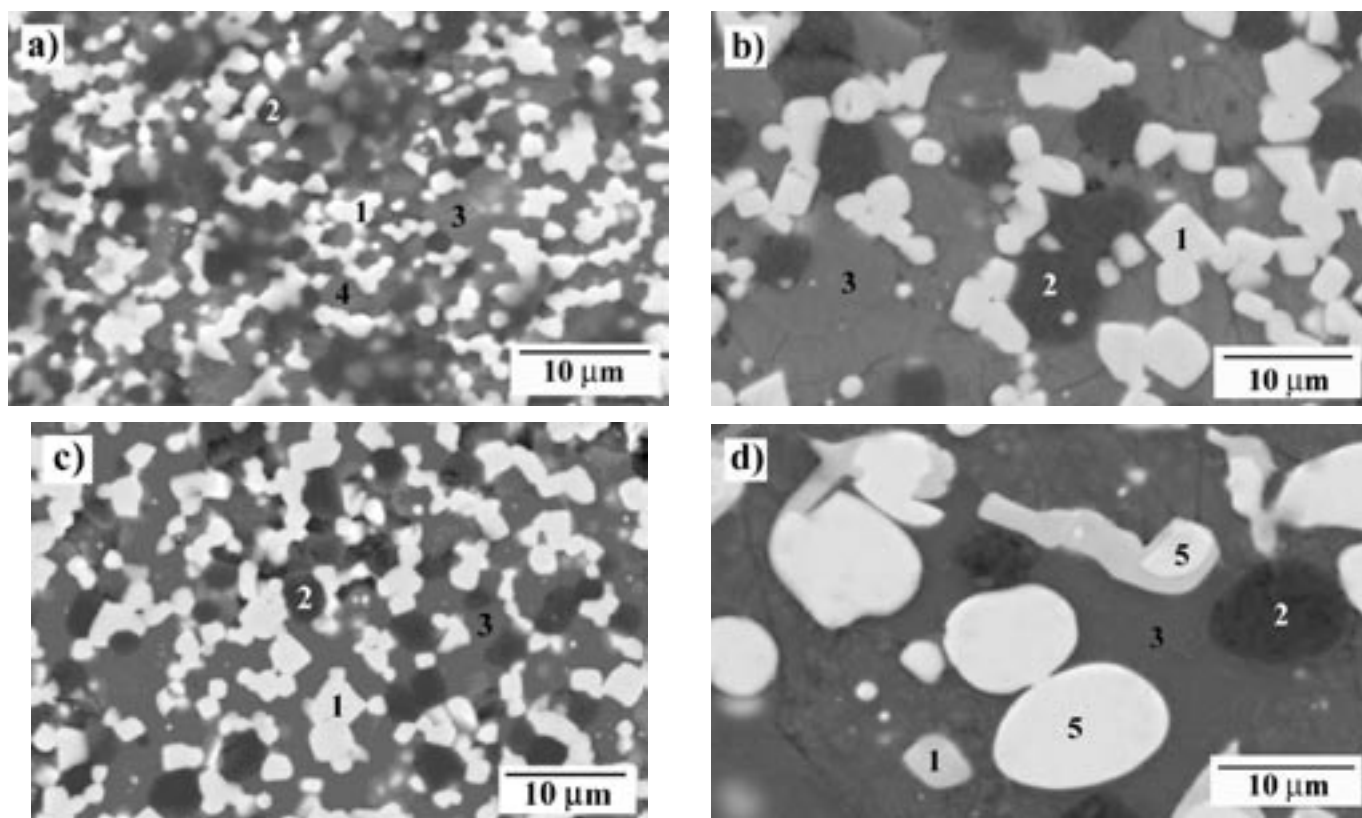


Fig. 4.- SEM BEI micrographs of samples of Region II sintered at 1550°C, with compositions (a) $X = 0$ and (b) $X = 1$, as well as of samples of Region III with compositions and sintering temperatures of (c) $X = 0$ and 1500°C, and (d) $X = 1$ and 1450°C.

Figs. 4c and 4d show micrographs of two samples of region III with molar compositions and sintering temperatures of $X = 0$ and 1500°C, and $X = 1$ and 1450°C, respectively. Sample of Fig. 4c shows a microstructure similar to that observed in the sample of Fig. 4a, except for the fact that the Ca_2SiO_4 phase is not present in the former specimen. Besides, the particle sizes of the CaZrO_3 , MgO and $\text{Ca}_3\text{Mg}(\text{SiO}_4)_2$ phases, which are 4.5, 3.7 and 6.3 μm , respectively, are larger for the case of the sample of Fig. 4c. On the other hand, the microstructure of sample of Fig. 4d is similar to that observed in the sample of Fig. 4b, except for the additional presence in the former specimen of phase 5, which has a white color, a rounded shape and a particle size ranging from 3 to 15 μm , and which correspond to ZrO_2 , according to the EDX analyses. It can be clearly appreciated that the formation of ZrO_2 takes place inside the particles of CaZrO_3 . Another important difference observed between both samples is a larger size (~ 5 -15 μm) and consequently a smaller number for the particles of CaZrO_3 and MgO in the sample of Fig. 4d with respect to the sample of Fig. 4b. For both samples of Figs. 4b and 4d, the matrix of the material is constituted by merwinite.

In general, the microstructural differences observed in the sintered samples of regions II and III are associated with differences in their chemical composition, due in part to the presence of an excess of calcite, as well as with differences in their sintering temperature. The excess of calcite resulted in an increase in the reaction kinetics by giving rise to the formation of phases with low melting point, mainly CaSiO_3 and $\text{Ca}_3\text{Mg}(\text{SiO}_4)_2$, which have melting points of 1544 and 1475°C, respectively. The latter temperature coincides with the invariant point for Region III. The appearance of these

phases originates the formation of transient liquids (12), which promote densification of the material and activate the growth of crystalline phases for composition $X = 1$ in both regions II and III. These inferences are in good agreement with the results shown in Figs. 4b and 4c, which have the same composition in different regions, i.e., the molar composition $X = 1$ in region II and the molar composition $X = 0$ in region III are located at the same point in the quaternary system, but they were sintered at different temperatures, 1550 and 1500°C, respectively. This difference of 50°C in the sintering temperature of samples 4b and 4c increases the amount of transitory liquid phase, affecting the size distribution, morphology and amount of the $\text{Ca}_3\text{Mg}(\text{SiO}_4)_2$, CaZrO_3 and MgO crystalline phases.

4. CONCLUSIONS

a) The reaction sintering of dolomite-zircon mixtures is a novel way to produce, in a single heat treatment step, dense polycrystalline MgO-CaZrO_3 - additional phase materials.

b) The weight loss of 47% corresponding to the stoichiometric dolomite, which is associated with the release of gaseous CO_2 , was increased to 66.1% for the Mexican dolomite due to an excess of 3% of CaCO_3 .

c) It is very important to take into account the excess of CaCO_3 in dolomite during the calculation of the studied formulations, because it has the effect of displacing the composition of the materials and their sintering temperature into other primary crystallization fields within the quaternary system.

d) A 3% in excess of CaCO_3 increases the amount of

CaZrO_3 , Ca_2SiO_4 and $\text{Ca}_3\text{Mg}(\text{SiO}_4)_2$ formed, while decreases the amount of free MgO .

e) The results are in good agreement with the predictions made based on the quaternary system $\text{CaO-MgO-SiO}_2\text{-ZrO}_2$.

5. ACKNOWLEDGEMENTS

The authors acknowledge the financial support of CINVESTAV and CONACYT (project number 39557-Y), both from México. Berenice Fernández-Arguijo thanks Eng. Felipe de Jesús Márquez-Torres of CINVESTAV-Salttillo for his assistance in the preparation of samples for SEM observations, as well as Eng. Carlos Palacios of Química del Rey, MET – MEX Peñoles, who supplied the dolomite used in this work.

REFERENCES

1. T. Hatfield, C. Richmond, W. Ford and J. White. "Relaciones de compatibilidad entre fases de periclasa y silicato en refractario de magnesita a altas temperaturas". *Bol. Soc. Esp. Ceram. V. 10*, 667-684 (1971).
2. A. Sircar, N.H. Brett and J. White. "Phase studies in the system $\text{CaO-MgO-ZrO}_2\text{-SiO}_2$, Part II: Compatibility relations of zirconia". *Trans. Brit. Ceram. Soc. 77*, 77-78 (1978).
3. Y. Suzuki, P. Morgan, T. Sekino and K. Niihara. "Manufacturing nanodiphasic materials from natural dolomite: In situ observation of nanophase formation behavior". *J. Am. Ceram. Soc. 80*, 2949-2953 (1997).
4. W. M. Kriven. "Possible alternative transformation toughening to zirconia: Crystallographic aspects". *J. Am. Ceram. Soc. 71*, 1021-1030 (1991).
5. S. De Aza, C. Richmond and J. White. "Compatibility relationships of periclasa in the system $\text{CaO-MgO-ZrO}_2\text{-SiO}_2$ ". *Trans. Brit. Ceram. Soc. 73*, 109-116 (1974).
6. P. Pena, B. A. Vázquez, A. Caballero, S. De Aza. "Diagramas de Equilibrio de fases cuaternarios. Métodos de representación e interpretación". *Bol. Soc. Esp. Ceram. V. 44* [2] 113-122 (2005).
7. D. W. Richardson. "Physical and thermal behavior", pp. 123-161 en *Modern Ceramic Engineering: Properties, Processing and Use in Design*, Marcel Dekker, New York (USA) 1992.
8. W.E. Lee and W.M. Rainforth. "Refractory materials", pp. 470-488 en *Ceramic Microstructures: Property Control by Processing*, Chapman & Hall, London (U.K.) 1994.
9. P.L. Fullman. "Measurement of particle sizes in opaque bodies". *Trans. Soc. AIME 197*, 447-452 (1953).
10. A. H. De Aza, M.A. Rodríguez, J.L. Rodríguez, S. De Aza, P. Pena and X. Turrillas. "The decomposition of dolomite monitored by neutron thermodiffractometry". *J. Am. Ceram. Soc. 85*, 881-888 (2002).
10. R. Otsuka. "Recent studies on the decomposition of the dolomite group by thermal analysis". *Thermochim. Acta 100*, 69-80 (1986).
11. J. L. Rodríguez, M. A. Rodríguez, S. De Aza and P. Pena. "Reaction sintering of zircon-dolomite mixtures". *J. Eur. Ceram. Soc. 21*, 343-354 (2001).
12. A. H. De Aza, X. Turrillas, J. L. Rodríguez, P. Pena. "Estudio del proceso de sinterización reactiva en sistemas con dolomita mediante termodiffractometría de neutrones". *Bol. Soc. Esp. Ceram. V. 43* [1] 12-15 (2004)

Recibido: 10.06.04

Aceptado: 30.03.05

